High performance liquid crystals for vehicle displays

Fenglin Peng,[1] Yuge Huang,[1] Fangwang Gou, [1] Minggang Hu,[1,2] Jian Li,[2] Zhongwei An,[2] and Shin-Tson Wu[1,*]

[1]College of Optics and Photonics, University of Central Florida, Orlando, Florida 32816, USA
[2]Xi'an Modern Chemistry Research Institute, Xi'an 710065, China
[*]swu@creol.ucf.edu

Abstract: We report three liquid crystal (LC) mixtures with a wide nematic range (−40°C to ~100°C), small visco-elastic coefficient and low activation energy for vehicular displays. Physical properties at different temperatures were characterized. These LCs greatly improve the performance of different display devices in a car: 1) for head-up projection using liquid-crystal-on-silicon with an average gray-to-gray (GTG) response time less than 1 ms at an elevated temperature. 2) The average GTG response time is maintained at ~10 ms for fringing field switching LCD at $T = 0$°C and also ~10 ms for twisted nematic LCD at $T = -20$°C.

©2016 Optical Society of America

OCIS codes: (160.3710) Liquid crystals; (230.3720) Liquid-crystal devices.

References and links

1. P. M. Knoll, "The use of displays in automotive applications," J. Soc. Inf. Disp. **5**(3), 165–172 (1997).
2. M. H. Schuck, D. J. McKnight, and K. M. Johnson, "Automotive head-up display using liquid-crystal-on-silicon displays," J. Soc. Inf. Disp. **5**(1), 33–35 (1997).
3. N. Takasaki, T. Harada, A. Sakaigawa, K. Sako, M. Mifune, and Y. Shiraishi, "Development of RGBW LCD with edge lit 2D local dimming system for automotive applications," SID Symp. Dig. Tech. Pap. **46**(1), 616–619 (2015).
4. S. T. Wu and C. S. Wu, "Mixed-mode twisted nematic liquid crystal cells for reflective displays," Appl. Phys. Lett. **68**(11), 1455–1457 (1996).
5. M. Schadt and W. Helfrich, "Voltage dependent optical activity of a twisted nematic liquid crystal," Appl. Phys. Lett. **18**(4), 127–128 (1971).
6. S. H. Lee, S. L. Lee, and H. Y. Kim, "Electro-optic characteristics and switching principle of a nematic liquid crystal cell controlled by fringe-field switching," Appl. Phys. Lett. **73**(20), 2881–2883 (1998).
7. Y. Chen, Z. Luo, F. Peng, and S.-T. Wu, "Fringe-field switching with a negative dielectric anisotropy liquid crystal," J. Display Technol. **9**(2), 74–77 (2013).
8. D. H. Kim, Y. J. Lim, D. E. Kim, H. Ren, S. H. Ahn, and S. H. Lee, "Past, present, and future of fringe-field switching-liquid crystal display," J. Inf. Disp. **15**(2), 99–106 (2014).
9. Z. Luo, F. Peng, H. Chen, M. Hu, J. Li, Z. An, and S.-T. Wu, "Fast-response liquid crystals for high image quality wearable displays," Opt. Mater. Express **5**(3), 603–610 (2015).
10. K.-H. Fan-Chiang, S.-T. Wu, and S.-H. Chen, "Fringing-field effects on high-resolution liquid crystal microdisplays," J. Display Technol. **1**(2), 304–313 (2005).
11. M. Schadt, M. Petrzilka, P. R. Gerber, A. Villiger, and G. Trickes, "New liquid crystal materials; physical properties and performance in displays for automobile, high information density and guest-host applications," Mol. Cryst. Liq. Cryst. (Phila. Pa.) **94**(1–2), 139–153 (1983).
12. M. Schadt, "Liquid crystal materials and liquid crystal displays," Annu. Rev. Mater. Sci. **27**(1), 305–379 (1997).
13. H. Chen, F. Peng, Z. Luo, D. Xu, S.-T. Wu, M.-C. Li, S.-L. Lee, and W.-C. Tsai, "High performance liquid crystal displays with a low dielectric constant material," Opt. Mater. Express **4**(11), 2262–2273 (2014).
14. Y. Iwata, M. Murata, K. Tanaka, T. Ohtake, H. Yoshida, and K. Miyachi, "Novel super fast response vertical alignment-liquid crystal display with extremely wide temperature range," J. Soc. Inf. Disp. **22**(1), 35–42 (2014).
15. F. Peng, H. Chen, S. Tripathi, R. J. Twieg, and S.-T. Wu, "Fast-response infrared phase modulator based on polymer network liquid crystal," Opt. Mater. Express **5**(2), 265–273 (2015).
16. F. Peng, Y.-H. Lee, H. Chen, Z. Li, A. E. Bostwick, R. J. Twieg, and S.-T. Wu, "Low absorption chlorinated liquid crystals for infrared applications," Opt. Mater. Express **5**(6), 1281–1288 (2015).
17. S. T. Wu, "Nematic liquid crystal modulator with response time less than 100 μs at room temperature," Appl. Phys. Lett. **57**(10), 986–988 (1990).

18. M. Schadt, R. Buchecker, and K. Müller, "Invited lecture. material properties, structural relations with molecular ensembles and electro-optical performance of new bicyclohexane liquid crystals in field-effect liquid crystal displays," Liq. Cryst. **5**(1), 293–312 (1989).
19. H. Chen, M. Hu, F. Peng, J. Li, Z. An, and S.-T. Wu, "Ultra-low viscosity liquid crystals," Opt. Mater. Express **5**(3), 655–660 (2015).
20. S.-T. Wu, U. Efron, and L. D. Hess, "Birefringence measurements of liquid crystals," Appl. Opt. **23**(21), 3911–3915 (1984).
21. I. Haller, "Thermodynamic and static properties of liquid crystals," Prog. Solid State Chem. **10**, 103–118 (1975).
22. S.-T. Wu, "Birefringence dispersions of liquid crystals," Phys. Rev. A **33**(2), 1270–1274 (1986).
23. S.-T. Wu and C.-S. Wu, "Experimental confirmation of the Osipov-Terentjev theory on the viscosity of nematic liquid crystals," Phys. Rev. A **42**(4), 2219–2227 (1990).
24. E. P. Raynes, "The theory of supertwist transitions," Mol. Cryst. Liq. Cryst. (Phila. Pa.) **4**(1), 1–8 (1986).
25. U. Finkenzeller and G. Weber, "A simple method to estimate and optimize the optical slope of TN-Cells and its comparison with experimental results," Mol. Cryst. Liq. Cryst. (Phila. Pa.) **164**(1), 145–156 (1988).
26. L. M. Blinov and V. Chigrinov, *Electrooptic Effects in Liquid Crystal Materials* (Springer-Verlag, 1994).
27. D. Xu, F. Peng, G. Tan, J. He, and S.-T. Wu, "A semi-empirical equation for the response time of in-plane switching liquid crystal display and measurement of twist elastic constant," J. Appl. Phys. **117**(20), 203103 (2015).
28. E. H. Stupp and M. S. Brennesholtz, *Projection Displays* (Wiley, 1999).
29. Y. Chen, F. Peng, and S.-T. Wu, "Submillisecond-response vertical-aligned liquid crystal for color sequential projection displays," J. Display Technol. **9**(2), 78–81 (2013).
30. K. H. Fan-Chiang, C. C. Yen, C. H. Wu, C. J. Chen, B. J. Liao, Y. Y. Ho, C. Y. Liu, and Y. C. Chen, "LCOS panel using novel color sequential technology," SID Int. Symp. Digest Tech. Papers **38**(1), 150–153 (2007).
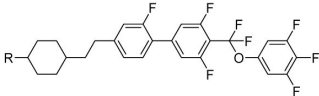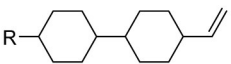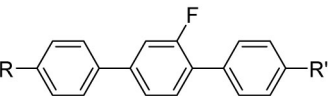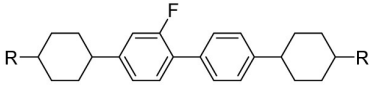
1. Introduction

Several liquid crystal display (LCD) devices have been widely used in a vehicle [1], such as head-up display (HUD) [2], wearable display, instrument cluster display, center information display, and entertainment display [3]. Mixed-mode twisted nematic (MTN) [4], twisted nematic (TN) [5] and fringe field switching (FFS) [6–8] are the main liquid crystal (LC) modes employed in the vehicular display system. For examples, 1) MTN is commonly used for liquid-crystal-on-silicon (LCOS) reflective projection displays (e.g. HUD and wearable displays) [9], since it exhibits high transmittance, low operation voltage and small fringing field effect [10]. 2) Transmissive TN LCD is employed in instrument cluster displays since the device requires fast response time and high brightness. The viewing angle of TN mode is relatively narrow. However, the instrument cluster display only shows information to the driver, thus narrow viewing angle is acceptable. 3) FFS LCD is applied to center information display (e.g. Global Positioning System (GPS)) and entertainment displays since information sharing, high image quality and touch panel are preferred for those displays. FFS mode shows advantages in wide view, weak color shift and pressure resistance for touch panels. However, there are two major challenges for vehicular displays in the extreme environment [11]: 1) it requires an LC with high clearing point (T_c ~100°C). For other LCD applications (e.g. TV, desktop and smartphones), a somewhat lower clearing point (~80°C) is still acceptable [12, 13]. While for displays inside a car, the temperature (T) could easily exceed 80°C during summer time. 2) The displays should remain operational at cold temperature, at least the LC should not freeze at −40°C, while keeping a reasonably fast response time below 0°C [14]. Because during winter time, the displays (e.g. the instrument cluster display and GPS) should remain functional before the car is warmed up. According to European car standard, the response time should be < 200ms at −20°C and < 300 ms at −30°C, respectively. But it is not fast enough to avoid image degradation. The general required operation temperature is from −30°C to 85°C and the storage temperature is from −40°C to 90°C for vehicle display applications. To boost clearing point, three-ring and four-ring LC compounds are commonly used, which dramatically increase the visco-elastic coefficient and activation energy [15, 16]. As a result, LC response time could be as sluggish as several hundreds of millisecond and the display image quality is severely degraded. For electric vehicles, low operation voltage is also very important considering the power consumption.

In this paper, we report three high performance LC mixtures with an extraordinary wide nematic range (−40°C to ~100°C), small visco-elastic coefficient, and low activation energy for automobile displays. Physical properties at different temperatures and wavelengths are characterized. We also explored these LC mixtures for different applications. For HUD projection display and wearable display, we obtain submillisecond average gray-to-gray (GTG) response time (~0.3 ms) in a MTN LCOS. By applying LCs to FFS and TN LCDs, the response time is less than 20 ms for FFS at 0°C and TN at −20°C, respectively. With overdrive voltage [17], the average GTG response time is further reduced by ~2X (< 10ms) at these low temperatures.

2. Experiment and results

Table 1 lists the chemical structures of compounds employed in the LC mixture, designated as MCRI. Four major ingredients are included. The homologues (different alkyl chain length R) of Compound 1 show high birefringence (Δn) and large dielectric anisotropy ($\Delta\varepsilon > 25$). However, their visco-elastic coefficient and activation energy are relatively large. To reduce viscosity, we doped ~50 wt% non-polar diluters (i.e. Compound 2 [18, 19]). Compounds 3 and 4 (~30 wt%) are added to obtain high clearing point (T_c) and wide nematic range. We also prepared other two LCs (designated as DIC-57F-15 and DIC-57F-16) with different visco-elastic constant and $\Delta\varepsilon$, which can be achieved by adjusting the concentration of non-polar diluters (Compound 2). The phase transition temperatures were measured by Differential Scanning Calorimetry (DSC, TA instruments Q100). Remarkably, the melting points (T_m) are below −40°C (due to the limit of our DSC) and T_c ~100°C for all three LCs, which show high durability in harsh environments. To determine $\Delta\varepsilon$, we measured the capacitance of a homogeneous and a homeotropic cell using an HP-4274 multi-frequency LCR meter. The measured phase transition temperatures and dielectric anisotropy of three LCs are summarized in Table 2.

Table 1. Chemical structures and compositions of our MCRI mixture.

Compounds #.	Chemical structure	wt %
1		25
2		48
3		18
4		9

2.1 Birefringence

To characterize the physical properties at different temperatures, we filled each LC into a homogeneous cell with cell gap (d ~5μm). A Merck mixture (MLC-6241-000) with similar T_c

(~99°C) was included as a benchmark for comparison. This is not the best mixture developed by Merck for practical applications but it is what we can find in our lab. The cells were mounted in a Linkam LTS 350 Large Area Heating/Freezing Stage controlled by TMS94 Temperature Programmer and then sandwiched between two crossed polarizers. A 1 kHz square-wave AC voltage was applied to LC cells. The probing light sources were a tunable Argon ion laser (λ = 457nm, 488nm, and 514nm) and a He-Ne laser (λ = 632.8 nm). The birefringence can be obtained from the phase retardation $\delta = 2\pi d\Delta n/\lambda$ [20]. We also measured their Δn at T = 10 ~90°C as Fig. 1(a) shows. The dots are experimental data and solid lines are theoretical fittings [21] with

$$\Delta n = \Delta n_o S = \Delta n_o (1 - T / T_c)^\beta, \tag{1}$$

where Δn_o is the extrapolated birefringence at T = 0K and the exponent β is a material constant. DIC-57F-15 shows a higher birefringence than other mixtures because it contains more compounds with a longer conjugation length (e.g. Compounds 1 and 3 in Table 1). High birefringence helps to reduce the required cell gap for achieving fast response time. The Δn of DIC-57F-16 and MCRI is ~0.1, which helps minimize the color dispersion of the LCD.
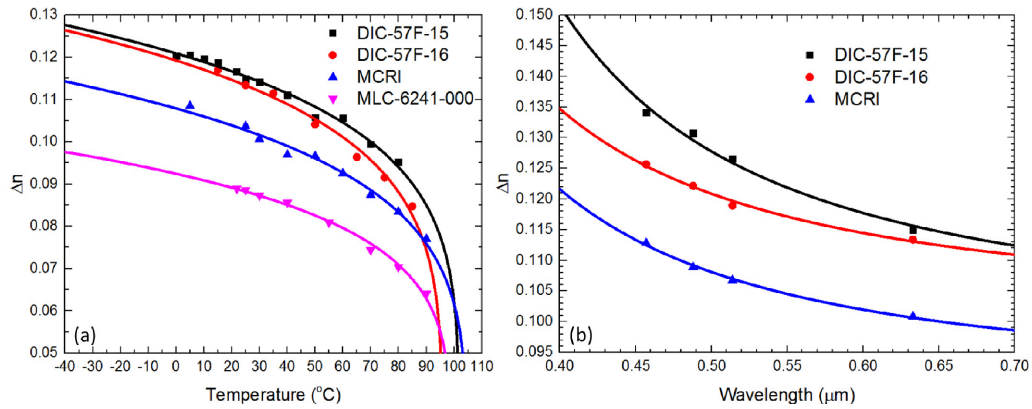

Fig. 1. (a) Temperature dependent birefringence and (b) dispersion curves at T = 25°C for the LC mixtures studied. Dots are measured data and solid lines are fitting curves with Eq. (1) and Eq. (2) in (a) and (b), respectively.

To investigate the electro-optic performance with different colors, we also fitted the measured Δn (dots in Fig. 1(b)) at each wavelength with the single-band dispersion equation [22]:

$$\Delta n = G \frac{\lambda^2 \lambda^{*2}}{\lambda^2 - \lambda^{*2}}. \tag{2}$$

Here, G is a proportionality constant and λ^* is the mean resonance wavelength. The fitting parameters in Fig. 1(a) and (b) are summarized in Table 3. Once G and λ^* are obtained, birefringence at any wavelength can be calculated from Eq. (2). Our results are: Δn = 0.122, 0.117 and 0.105 at λ = 550nm for DIC-57F-15, DIC-57F-16 and MCRI, respectively. These values are included in Table 2 and will be used in the device simulation later.

Table 2. Physical properties of four LC mixtures at _T_ = 25°C.

LC mixture	T_m (°C)	T_c (°C)	$\Delta\varepsilon$	Δn ($\lambda = 550nm$)	K_{11} (pN)	γ_1 (mPaS)	K_{22} (pN)
DIC-57F-15	< −40	102	5.0	0.122	12.9	70.5	7.7
DIC-57F-16	< −40	97	4.4	0.117	11.9	63.4	7.3
MCRI	< −40	104	4.0	0.105	12.0	55.3	4.7
MLC-6241-000	-	99	5.5	0.090	13.8	133.5	7.5

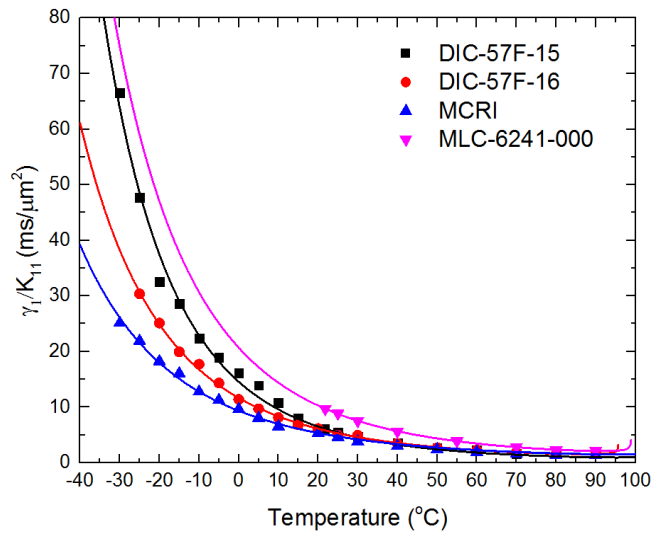## 2.2 Visco-elastic coefficient

Fig. 2. Temperature dependent visco-elastic coefficients. Dots are experimental data and solid lines are the fitting curves with Eq. (3).

From the response time measurement, we can extract the visco-elastic coefficient (γ_1/K_{11}) of the LC mixture [23]. Figure 2 depicts the γ_1/K_{11} from −30°C to 90°C, in which dots represent experimental data. As the temperature decreases, γ_1/K_{11} increases exponentially. The solid lines are the fitting curves with following equation:

$$\frac{\gamma_1}{K_{11}} = A \frac{\exp(E_a / k_B T)}{(1 - T / T_c)^\beta}.$$

(3)

In Eq. (3), A is a proportionality constant, k_B is the Boltzmann constant, E_a is the activation energy, and β is the material constant, which has been obtained through Eq. (2). Table 3 lists the fitting parameters for all four LC mixtures studied. Our new LCs exhibit a smaller γ_1/K_{11} than MLC-6241-000 at any temperature. Besides, the new LCs have similar γ_1/K_{11} at $T\sim35°C$. However, MCRI has the smallest activation energy and slowest rising rate as the temperature decreases. The activation energy (E_a) is affected by several parameters such as molecular

structure and conformation, and intermolecular interactions [23]. To reduce the viscosity at room temperature, MCRI employs a higher concentration of non-polar diluters (Compound 2 in Table 1). As a result, its E_a is relatively small, which in turn contributes to a mild increase of visco-elastic coefficients, as described in Eq. (3). Therefore, the visco-elastic coefficient of MCRI is the smallest at low temperature. While, DIC-57F-15 exhibits a smaller γ_1/K_{11} at T > 35°C due to a larger activation energy. So its γ_1/K_{11} deceases dramatically at elevated temperatures. Therefore, DIC-57F-16 and MCRI show better performance especially faster response time at low temperatures. The response time is proportional to γ_1/K_{11} and d^2. DIC-57F-15 shows the highest $\varDelta$n among four LCs. As a result, the required cell gap of DIC-57F-15 is the thinnest to achieve the same phase retardation. With a thinner cell gap and smaller γ_1/K_{11} at elevated temperatures, DIC-57-15 is more suitable for projection displays, whose operation temperature is 35-55°C, depending on the employed light source (LED or arc lamp). We will discuss their applications later.

Table 3. Fitting parameters of the four LC mixtures at T = 25°C.

LC mixture	Δn_0	β	G (μm^{-2})	$\lambda*$ (μm)	A ($ms/\mu m^2$)	E_a (meV)
DIC-57F-15	0.15	0.16	1.83	0.23	5.26×10^{-5}	290.3
DIC-57F-16	0.15	0.17	2.64	0.20	4.23×10^{-4}	235.7
MCRI	0.14	0.18	2.19	0.20	1.24×10^{-3}	204.9
MLC-6241-000	0.11	0.16	-	-	3.54×10^{-4}	253.7

2.3 Elastic constants K_{11} and K_{22}

Elastic constants affect the threshold voltage and response time of a LC device. For the above mentioned MTN, TN and FFS LCDs, splay (K_{11}) and twist (K_{22}) elastic constants are more important than the bend (K_{33}). We measured K_{11} from the threshold voltage (V_{th}) based on the voltage-dependent transmittance (VT) curve since V_{th} is expressed as [24–26]:

$$V_{th} = \pi \sqrt{\frac{K_{11}}{\varepsilon_0 \Delta \varepsilon}}, \tag{4}$$

where ε_0 is the permittivity of free space. Because γ_1/K_{11} has been obtained by measuring the free relaxation time, we can extract the rotational viscosity (γ_1) easily. Results are also included in Table 2.

To obtain K_{22}, Xu et al. [27] derived following semi-empirical equation to describe the optical decay time of an In-Plane Switching (IPS) cell:

$$\tau_d = 1.238 \bullet \frac{\gamma_1 d^2}{K_{22} \pi^2}. \tag{5}$$

In experiment, we prepared four IPS cells whose substrates were coated with a thin polyimide (PI) layer to provide strong anchoring energy. The cells were sandwiched between two crossed linear polarizers with the bottom polarizer's transmission axis parallel to the LC rubbing direction. First, we measured the VT curve of each mixture at T = 25°C and biased the LC cell at peak transmission voltage. Then we removed the bias voltage instantaneously and recorded the transient decay time with a digital oscilloscope. Using Eq. (5), we can calculate K_{22}. Results are also listed in Table 2.

2.4 Discussion

As Table 2 shows, a smaller $\Delta\varepsilon$ mixture tends to have a lower γ_1 because it consists of a higher concentration of diluters (compound 2 in Table 1). Diluters are nonpolar short-chain compounds with a very low viscosity. There is a linear relationship between $\Delta\varepsilon$ and γ_1 for LCs with T_c ~80°C and Δn~0.1 [19]. These LCs have been widely used in TVs, smartphones and wearable displays. Figure 3 depicts the dielectric anisotropy ($\Delta\varepsilon$) vs. rotational viscosity (γ_1) of several positive (+) and negative (−) $\Delta\varepsilon$ LCs with $T_c \approx 80$°C and $T_c \approx 100$°C. All three kinds of LCs show linear relationship between $|\Delta\varepsilon|$ and γ_1. The extrapolated $\gamma_1 = 30$ mPas when $\Delta\varepsilon \rightarrow 0$, which represents the γ_1 of the nonpolar diluters. With a similar T_c, $|\Delta\varepsilon|$ and Δn, $-\Delta\varepsilon$ LC shows a much higher rotational viscosity than that of $+\Delta\varepsilon$ LC. This is because more dipole groups are needed for a $-\Delta\varepsilon$ LC to achieve the same $|\Delta\varepsilon|$ as a $+\Delta\varepsilon$ LC. As a result, the compound becomes bulkier and heavier, leading to a higher rotational viscosity. On the other hand, to increase the clearing point of a $+\Delta\varepsilon$ LC mixture, more three- or four-ring structures (e.g. Compounds 3 and 4 in Table 1) are required. Thus, a $+\Delta\varepsilon$ LC with a higher T_c often exhibits a larger γ_1.
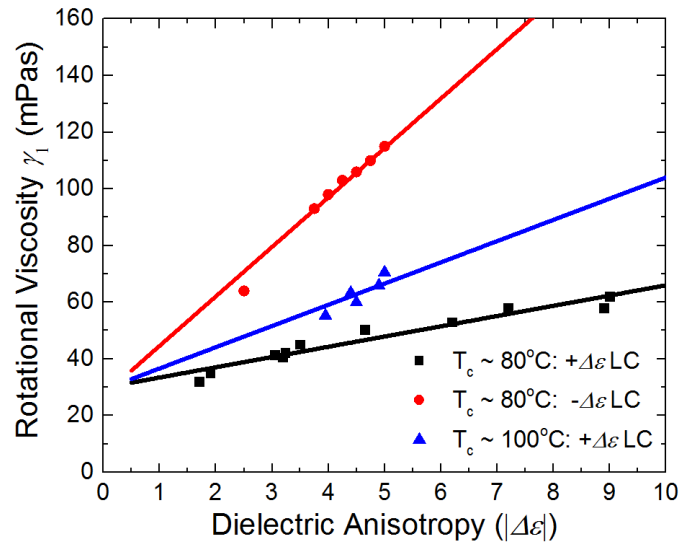

Fig. 3. Dielectric anisotropy ($\Delta\varepsilon$) vs. rotational viscosity at $T = 25$°C.

3. Device simulation results

3.1 Submillisecond-response color sequential projection displays

Color sequential LCOS has been widely used in projection displays [28–30] and wearable displays, such as Google Glass. By eliminating the color filters, both resolution density and brightness are tripled. However, fast response time (< 1 ms) is required to suppress the color breakup and keep high image quality. Besides, the LCOS panel could operate at $T = 35$-55°C due to thermal effect from the high power arc lamp or LED.

As Fig. 2 depicts, DIC-57F-15 shows the lowest visco-elastic coefficient and it requires the thinnest cell gap (i.e. highest birefringence) when $T > 35$°C. Therefore, we use a commercial LCD simulator DIMOS 2.0 to calculate the electro-optic properties of a MTN-LCOS with DIC-57F-15. In a MTN cell, the LC directors are twisted by 90° from top to bottom substrates (i.e. MTN-90°). From Fig. 1(a) and (b) and fitting parameters (Table 3), we found that at $T = 55$°C, $\Delta n = 0.112$ at $\lambda = 550$ nm. The measured $\Delta\varepsilon$ is 4.7 at $T = 55$°C. The other simulation parameters were set as $d = 1.95$ μm and $\gamma_1/K_{11} = 2.10$ ms/μm^2 for $T = 55$°C. The angle between front LC directors and the PBS polarization axis is set at 20° to maximize

the reflectance and the initial pretilt angle is ~2°. MTN-90° modulates the light reflectance by a mixed effect between polarization rotation and phase retardation. A reflector is placed on the inner surface of the MTN-90° cell. For blue (B) and red (R) lights, we used $\Delta n = 0.112$ and 0.105, respectively, while keeping the same cell gap. Figure 4 depicts the voltage-dependent reflectance (VR) curves for the RGB colors. A good dark state is achieved at V ≈4.5 V_{rms}. Thus, only single gamma curve is needed for driving the RGB frames.

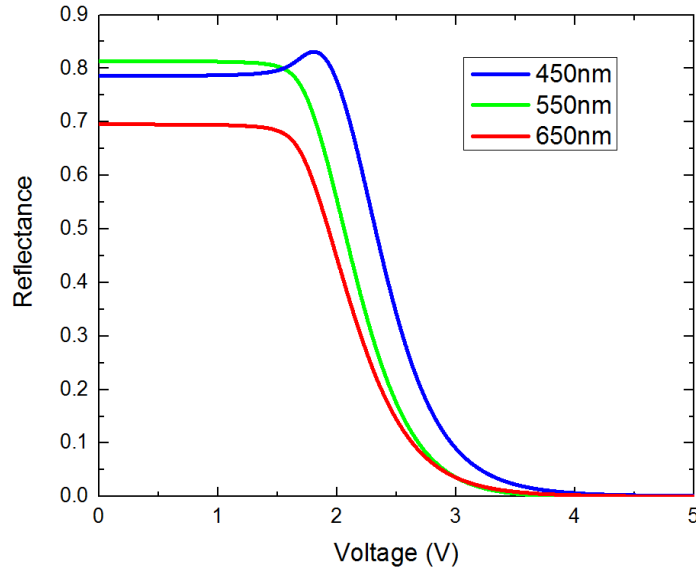Fig. 4. Voltage-dependent reflectance curves for R, G, B colors. The cell gap is 1.95 μm and T = 55 °C

Table 4 summarizes the calculated gray-to-gray (GTG) response time. Here, we divided the VR curve at λ = 550 nm into 8 gray levels and calculated the response time between different gray levels. Both rise time and decay time are defined as 10%-90% reflectance change. The calculated rise time is 1.00 ms and decay time is 0.43 ms between gray levels 1 and 8. By applying overdrive voltage, we obtained average GTG rise time is 0.50 ms and decay time is 0.20 ms, which are ~2X faster than the response time between gray levels 1 and 8. For projection displays using LED light sources, the chasis temperature is ~35°C. Based on Fig. 2, the extrapolated GTG rise time is ~1.00 ms and decay time ~0.40 ms. Such a fast response time would eliminate the color breakup of the color sequential LCOS projection display.

Table 4. Calculated GTG response time (ms) of the MTN cell using DIC-57F-15: d = 1.95μm and T = 55°C.

	1	2	3	4	5	6	7	8
1		0.23	0.30	0.37	0.46	0.56	0.71	1.00
2	0.25		0.13	0.24	0.35	0.47	0.64	0.97
3	0.29	0.08		0.12	0.23	0.37	0.55	0.94
4	0.30	0.13	0.06		0.13	0.27	0.47	0.91
5	0.31	0.17	0.10	0.05		0.15	0.36	0.90
6	0.33	0.21	0.15	0.10	0.05		0.23	0.89
7	0.36	0.25	0.20	0.15	0.11	0.07		0.92
8	0.43	0.34	0.29	0.26	0.24	0.22	0.20	

3.2 Fast-response TN and FFS LCDs at extreme environments

Here, we simulate the electro-optic properties of FFS and TN cells employing DIC-57F-16 and MCRI with a commercial LCD simulator DIMOS.2D, as these two LCs show small visco-elastic coefficients at T < 35°C and low activation energy. According to the dispersion curve, Δn ~0.12 and 0.11 for DIC-57F-16 and MCRI at λ = 550 nm. For MLC-6241-000, the estimated Δn ~ 0.09 at λ = 550nm. For FFS mode, we set $d\Delta n$ ~340 nm for each mixture in order to achieve fast response time and low operation voltage. The same cell parameters are used in the simulation for fair comparison: electrode width w = 2μm, electrode gap l = 3μm, pretilt angle ~2° and rubbing angle ~10°. For TN mode, $d\Delta n$ = 480 nm to satisfy first Gooch-Tarry minimum and to achieve high transmittance. The cells are sandwiched between two crossed polarizers and front rubbing direction is parallel to the axis of polarizer. Figures 5(a) and 5(c) depict the voltage-dependent transmittance for FFS and TN cells, respectively. In both modes, MLC-6241-000 shows the lowest operation voltage due to its largest $\Delta\varepsilon$. The on-state voltage of DIC-57F-16 is 6.0 V_{rms} and MCRI is 6.5 V_{rms} in FFS mode, which are still acceptable for vehicular displays. For TN, a good dark state is obtained at V~5 V_{rms} for both new LCs. Figures 5(b) and 5(d) depict the response time of FFS and TN LCDs at T = 25°C. The time-dependent transmittance curves of two newly developed LCs are almost the same because of their similar birefringence and visco-elastic coefficient. The response time of our LCs is much faster than that of MLC-6241-000 in both modes. Moreover, the faster response time contributes to a higher overall transmittance and lower image crosstalk. For FFS mode, the response time [rise, decay] of DIC-57F-16 is [9.7ms, 9.3ms], while the response time of MLC-6241-000 is [31.3ms, 31.2ms]. TN shows faster response time than FFS because it utilizes K_{11} while FFS mainly uses K_{22}. Thus, the response time of our LCs is [2.5ms, 5.0ms] for TN, which is ~3.6X faster than that of MLC-6241-000 ([9.0ms, 19.0ms]).
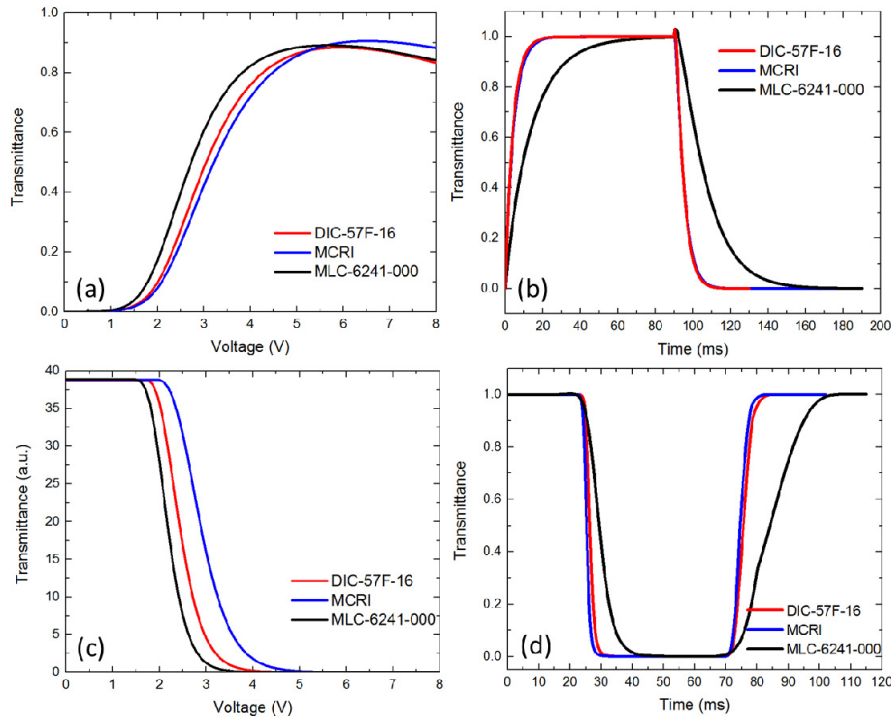

Fig. 5. (a) Voltage-dependent transmittance (VT) curves and (b) time-dependent transmittance (TT) curves for FFS mode at λ = 550nm; $d\Delta$n = 340nm. (c) VT curves and (d) TT curves for TN mode at λ = 550nm; $d\Delta$n = 480nm at T = 25 °C.

Based on Fig. 2, the response time at low temperature can be calculated. Table 5 shows the free relaxation time of FFS and TN modes at low temperatures. Our new LCs show a favorably small activation energy, leading to a much slower rising rate on visco-elastic coefficient as the temperature decreases. At 0°C, the extrapolated decay time of MCRI in FFS cell is still within 20ms, which is ~3.8X faster than that of MLC-6241-000. Besides, the rise time (i.e. free relaxation) of TN with MCRI is less than 20ms at $T = -20$°C (for MLC-6241-000, it is longer than 100ms). Thus, the response time of TN mode is >10X faster than that European car standard requires (i.e. 200ms at −20°C and 300ms at −30°C). By applying the overdrive voltage, the average GTG response time is reduced by ~2X. Therefore, by employing our new LCs, the response time is within ~10ms for FFS at $T = 0$°C and TN at $T = -20$°C. This is particularly important for vehicular displays at cold weather.

Table 5. The free relaxation time (ms) of FFS and TN modes at low temperature regions.

		25°C	0°C	−20°C	−30°C
FFS mode	DIC-57F-16	9.3	20.0	43.6	67.3
	MCRI	9.3	19.2	36.9	53.6
	MLC-6241-000	31.2	73.6	166.3	266.4
TN mode	DIC-57F-16	5.0	11.0	23.4	36.2
	MCRI	5.0	9.9	19.0	27.7
	MLC-6241-000	19.0	44.8	101.3	162.2

4. Conclusion

We have developed and characterized 3 new nematic LC mixtures with high clearing point, small visco-elastic coefficient and low activation energy. With a wide nematic range, they can meet the challenges for harsh environments of vehicular displays. By applying these mixtures to different LCD modes, we obtain following attractive features: 1) the average GTG response time is < 1ms with MTN mode for HUD and wearable displays at $T > 35$ °C. 2) The average GTG response time is maintained very fast (<10ms) for FFS at $T = 0$ °C and TN at $T = -20$ °C. As Table 5 shows, there are still some technical challenges for vehicle displays, such as faster response time at low temperatures for reducing image blurs, high ambient contrast ratio for daylight operations, and high transmittance for high brightness and low power consumption.

Acknowledgments